ZEOLITE SUPPORTED PALLADIUM NANOPARTICLE CHARACTERISATION FOR FUEL CELL APPLICATION

Jun Yao[1] and Yufeng Yao[2]

[1] School of Engineering, University of Lincoln, Brayford Pool, Lincoln LN6 7TS, UK, jyao@lincoln.ac.uk

[2] Department of Engineering Design and Mathematics, University of the West of England, Coldharbour Lane, Bristol BS16 1QY, UK, Yufeng.Yao@uwe.ac.uk

Highlights:

- Quantify electrochemical activity of Pd nanoparticle in electrolyte solution by CV.
- Characterise detailed local structure of Pd cluster by X-ray based EXAFS technique.
- Measure Pd nanoparticle size on Y-zeolite under different pre-treatment conditions.
- Explore up-hill diffusion process and surface conductance pathways on Pd surface.
- Discuss electrochemical reaction behaviour on Pd surface and Pt particle size.

Abstract:

Palladium (Pd) has been widely used as a type of hydrogen storage material and has attracted much attention for fuel cell applications, due to its high solubility and mobility of hydrogen in Pd. In this study, Pd nanoparticles made by 1.5 wt% Pd loading on Y-zeolite under pre-treatment was employed to investigate their electrochemical activities using cyclic voltammetry (CV), and detailed local structural characterization of Pd cluster was probed by the extended X-ray absorption fine structure. Pd nanoparticle sizes were predicted at 0.81nm - 1.2nm and the CV measurement has demonstrated that Pd zeolite catalyst has exhibited a similar tendency to those 40% Pd on XC-72R carbon. The hydrogen spillover process and surface conductance pathways contribute to the electrochemical behaviour on Pd surface. In electrochemical environment, hydrogen is able to form hydride phase on Pd surface by either direct hydrogen adsorption or migrating to the centre of Pd.

Keywords: Zeolite supported palladium nanoparticle; EXAFS and CV techniques; Fuel cell application.

1. Introduction

Over the past decades, Platinum (Pt) based materials used as electrocatalysts have been the most popular choices for direct methanol fuel cell application, due to their high activity and stability properties. However, the expensive cost and insufficient supplement of Pt have motivated researchers to develop and explore other alternative fuel cell electrocatalysts at a relatively lower cost with a comparable performance as to the Pt based catalyst system. Palladium (Pd) as one of the Pt-group metals has attracted significant attentions of research, since it has shown a relatively good activity for hydrogen oxidation reaction (HOR) and oxygen reduction reaction (ORR) in fuel cell applications [1, 2]. Moreover, Pd has been widely used in gas sensors and also as a hydrogen storage material [3, 4], owing to its capability of bulk incorporation of hydrogen which leads to the high solubility and mobility in Pd. Economically, the price of Pd is considerably cheaper at about two-thirds of the cost than that accounted for Pt. Therefore, Pd has been regarded as a compatible alternative substitute to Pt, if the electrocatalytic performance of Pd can be enhanced somehow, similar to that of Pt.

The direct methanol fuel cell presents some advantages over the pure hydrogen polymer fuel cell, as methanol is cheaper to produce and can be stored and distributed safely in comparison to hydrogen. However, the main weakness hindering it to be widely used is the lower fuel cell efficiency due to several reasons, including CO poisoning effect by blocking of the Pt active surface and the high over-potential during electro-oxidation process. By contrast, Pd based electrocatalyst shows some resilience to CO poisoning and has a relatively higher electrocatalytic activity for methanol electro-oxidation than Pt based electrocatalyst [5]. Recently, a lot of effort has been made to develop more electrochemical efficient Pd electrocatalyst by focusing on carbon based Pd catalyst system (e.g. carbon black, carbon nanotubes and graphene [6]) using various approaches such as composition control and developing of synthetic methods (e.g. electrochemical deposition [7] and spontaneous deposition [8]) to achieve high Pd utilization for different nanoparticle sizes and their

distributions. As Pd electrocatalytic activity is generally lower than Pt [9], most studies have focused on Pd alloy synthesis using metals such as Ni, Ag, C, Mo and Pt to produce novel nanostructure, i.e. core-shell, porous and shape controlled nanoparticles by de-alloying process using acid [1]. So far, few studies have been carried out to investigate Pd nanostructure and surface activity by employing polymer material such as zeolite, because its substrate comprising amorphous aluminosilicates structure. Therefore, this paper will focus on experimental study of zeolite supported Pd nanoparticle characteristics to realize its potential for fuel cell application.

Zeolite has presented a unique prosperity of high exchange capability and crystalline structure formed by Al-O-Si, which can assist the preparation of high dispersed metal particles by using fewer amounts of catalyst loading to produce different particle sizes [6, 10]. It was reported that the activity and stability of Pd based catalyst system can be improved by Pd nanoparticle and support interaction [11, 12]. Similar properties will be investigated in present study using a zeolite supported Pt nanoparticle (0.9 nm - 1.5 nm) catalyst system.

For noble metal based fuel cell electrocatalysts, Pt ions are much more stable in small cages such as zeolite sodalite cages or hexagonal prisms even under a high reduction temperature of 500 ^{o}C, due to the formation of large Pt particle size with high polarization ability attributed by the Pt d bond electron configuration [13]. However, Pd appears to be more mobile than Pt, and the locations of Pd on zeolite cages are found strongly dependent on calcinations and reduction temperature [10].

Tzou *et al.* [14] and Xu *et al.* [15] have reported their studies of Pd locations on zeolite under temperature control. In the process, Pd ions coordinated with one or two ammonia ligands can migrate into zeolite sodalite cages at 300 ^{o}C. Pd ions can be completely removed at calculation temperature up to 500 ^{o}C with some Pd ions found to occupy the hexagonal prisms. By increasing the reduction temperature is able to facilitate Pd atoms migrating from supercages to sodalite cages to form multi-atomic particles [15]. The majority of Pd could be released from sodalite cages to

74 supercages by hydrogen reduction at 350 ^{o}C [14]. At reduction temperature higher than 350 ^{o}C, it
75 was also reported to force Pd atoms migrating from the hexagonal prisms to the supercages [14].

76 The Pd migration process between zeolite cages can be critical to facilitate the increase of Pd
77 dispersion on zeolite, where small particles will act as nucleation sites to form new particle in
78 supercages. However, there are few literatures in public domain that have presented such studies to
79 explore Pd performance, i.e. the particle size and dispersion on zeolite in an electrochemical
80 environment, whereas most studies were merely focused on carbon or gold (Au) based Pd
81 electrocatalyst. One previous study by Zhao *et al.* [16] indicated that an average Pd particle size on
82 carbon can be between 2.7 nm and 5.2 nm, dependent on the process of catalyst pre-treatment. The
83 average Pd particle size of 6.6 nm to 30.3 nm has also been reported by coating Pd on microcellular
84 graphitic carbon foam as substrate with a lattice constant of 3.9 Å for face centered cubic (FCC)
85 structure, corresponding to a 5.0 % Pd loading on carbon foam [17]. Further studies using Pd L_3 X-
86 ray Adsorption Spectroscopy (XAS) method [18, 19] confirmed that the change of electronic and
87 geometric structure can alters Pd d bond observed on Pd, Cu and Pt based alloy electrocatalysts,
88 primarily due to the charge transfer among the neighboring metal atoms and interacted substrates.

89 Previously, the electrochemical activity of Pd in acid solution such as H_2SO_4 has been
90 reported on Au supported Pd catalyst system to determine the hydrogen evaluation and reduction
91 (HER) activity [20]. The exchange current density over Pd increases with the decrease of Pd overlays
92 on Au, owing to the strong adsorption energy of H_{ad}. Moreover, the HER activity increases with the
93 decrease of Pd coverage for systems in which the surface is decorated by a Pd cluster. Therefore, Pd
94 electrocatalyst morphology is believed to have played a substantial role in the HER performance
95 [21]. Further study [22] found that the preferred adsorption site for H_{ad} is identified at the hollow
96 FCC site by three Pd atoms for a Pd cluster, resulting in a low coverage of H_{ad}. A spillover and surface
97 diffusion process of adsorbed hydrogen atoms on Au surface is responsible for enhancing the HER
98 activity on Pd, as suggested by Pandelov and Stimming [23], and the hydrogen oxidation reaction

follows a similar pathway [24]. This is consistent to that has been discussed previously by present authors for hydrogen spillover and surface diffusion and conductance pathway on Pt nanoparticle catalyst system [25], since they share similar electronic properties. Nevertheless, the Pd specific activities such as oxidation and reduction reaction activity in acid solution are generally regarded lower than that of Pt, owing to the strong oxygen binding energy on Pd surface [24, 26, 27]. The strong dependence of Pd crystalline orientation can be a key consideration for electrochemical activities in acidic solution [28]. The Pd high specific activity was also demonstrated for Pd cubic particle size at 5nm - 6 nm, compared to that of Pd with an octahedral structure [29].

In present study, laboratory made zeolite supported 1.5 wt% Pd nanoparticle structure will be investigated by ion exchange method under various calcinations and reduction temperatures. Based on the outcome of previous study [14], ion exchange method can produce uniform Pd distribution within zeolite structures. The Pd electrochemical activity in hydride region will be determined under various potential depositions at -0.675 V, -0.65 V, and ±0.5 V in H_2SO_4 acidic solution, respectively. The oxygen reduction reaction will also be investigated with a potential swept up to 0.4 V, as Pd has shown a generally improved electrocatalytic activity for oxygen reduction reaction and hydrogen oxidation reaction [30]. Pd particle size and its dispersion on zeolite are to be characterized by cyclic voltammetry (CV) and the extended X-ray adsorption fine structure (EXAFS) techniques using a Nafion$^{@}$ bound electrode, fabricated by Pd/zeolite and carbon powder mixed with Nafion$^{@}$ to form ultra-thin film and membrane on electrode surface [31, 32]. The study will contribute to the understanding of the relation of electrochemical activity with correspondent to Pd particle size, and moreover, Pd and zeolite conducting pathway for the enhancement of the electrochemical activity, resulted by charger/electron transfer occurred at electrode and solution interface, since the activity of electrocatalyst is known to be mainly a surface property [33].

2. Experimental

2.1. The preparation of Pd/Y zeolite electrocatalysts

1.5 wt% Pd loading on Y zeolite electrocatalyst was made by ion exchange method [24, 25, 34] using $(NH_3)_4PdCl_4$ to achieve highly dispersed Pd with uniform distribution [14, 35]. The mechanism of ion replacement on zeolite is to exchange $[Pd(NH_3)_4]^{4+}$ ligand with sodium ion (Na^+) that has an affinity with a negative charge situated on the alumina tetrahedral arrangement $[AlO_4]^-$. One $[Pd(NH_3)_4]^{4+}$ ligand replaces four Na^+ ions to interact with four negative charges situated on four $[AlO_4]^-$ ions to make a charge balance. Then, one Pt^{4+} ion bridges four $[AlO_4]^-$ ions after calcination process to decompose ammonia ligand.

The ion exchange procedure was identical to that illustrated for Pt zeolite ion exchange process [25, 34]. The ion exchange was carried out in a neutral solution at pH 7. An appreciate quantity of $[Pd(NH_3)]_4Cl_4$ was dissolved in 200 ml of triply distilled water at 0.004 mol dm^{-3} in an ultrasonic bath at room temperature. The ion exchange process of Pd ions within zeolite was taken place in a water-jacketed reactor at 70 ^oC by dispersion of Y zeolite powder at a concentration of 1 g per 100 ml of triply distilled water. The Pd ions were added slowly by pumping the Pd salt solution at 0.1 ml min^{-1}. Then Pd Y zeolite sample was washed with a sufficient amount of triply distilled water until no $[Pd(NH_3)_4]^{4+}$ complex detected by Ultraviolet UV spectrum [25, 34], and the filtrate was tested using 1 N $AgNO_3$ to ensure the free of Cl^- ions. Subsequently, the sample was dried at a temperature of 120^oC in an oven.

The synthesis of Pd nanostructures on Y zeolite was carried out using calcinations and reduction procedure to remove Pd coordinate ligand. $[Pd(NH_3)_4]^{4+}$ salt/Y zeolite samples were purged with argon at 150 ^oC in a fluidized bed reactor to dry out the water moisture. After cooling, O_2 was introduced into the reactor to slowly re-heat samples up to 350 ^oC with O_2 purge at 200 ml/min. Then, samples were chemically reduced at 360 ^oC by purging with 5% H_2 and 95% N_2 gas mixture to produce a fine Pd distribution on zeolite (donated as 15Ptanc35r36). Figure 1 illustrates $[Pd(NH_3)_4]^{4+}$

ions decomposition process to produce the metallic Pd atoms that extend throughout zeolite cages under different level of calcinations and reduction temperatures. $[Pd(NH_3)_4]^{4+}$ ions are mainly located at zeolite exterior surface and supercgaes after ion exchange process. The ammonia ligands attached to Pd starts to decompose at 250 ^{o}C [10], and the Pd ions can migrate through zeolite channels and extend several cages of zeolite such as sodalite cages and hexagonal prism [35] under calculations and reduction temperature up to 300 ^{o}C. The Pd atoms migrate back to zeolite supercages and zeolite exterior surface under calcinations of 350 ^{o}C and reduction temperature of 360 ^{o}C, respectively. The following equations illustrate Pd ligand decomposition and Pd oxidation and reduction process.

Oxidation:

$$[Pd(NH_3)_4]^{4+} = NH_3\ (gas) + Pd^{4+}$$

$$O_2\ (gas) + Pd^{4+} = PdO_2$$

Reduction:

$$PdO_2 + 2H_2\ (gas) = 2H_2O + Pd$$

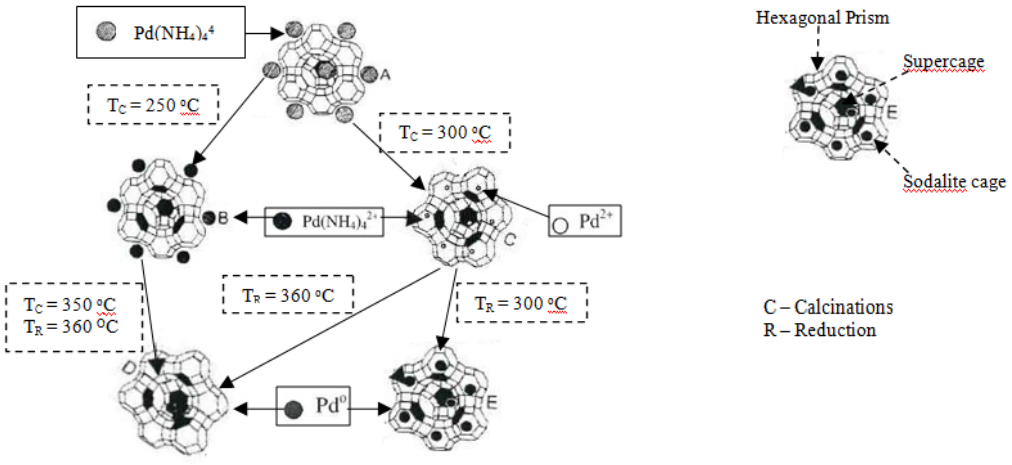

Figure 1. Schematic illustration of Pd location during calcinations and reduction process after ion exchange of $[Pd(NH_3)_4]^{4+}$ ions within zeolite.

2.2. Electrochemical Cell and Cyclic Voltammetry (CV)

The electrode was made of 1.5 wt% Pd loading on zeolite electrocatalyst and XC-72R carbon powder (untreated) mixed with 15 wt% Nafion$^{@}$ solution (i.e. 5 wt% solution in Aliphatic Alcohols and H_2O from Aldrich) as a binder (donated as 15Pdanc35r36). The resultant paste was then hot pressed on a sheet of 9 cm^2 carbon paper (E-TEK TGHP-90) for solidification. A disc of 2.5 cm^2 diameter of electrodes was then trimmed for CV measurement and a disc of 1.3 cm^2 for in-situ EXAFS measurement, respectively. A 40 wt% Pd/C or 1.5 wt% Pd/C made by 40 wt% Pd and extra XC-72R carbon mixture was employed to justify the CV results determined by 1.5 wt% Pd zeolite electrode, respectively.

The charge separation on electrode was investigated in a glass-jacketed electrochemical cell, consisting of a working electrode, Hg/Hg_2SO_4 Mercury/Mercuries Sulphate (MMS) reference electrode and a Pd gauze counter electrode. The in-situ EXAFS measurement was carried out in an electrochemical cell formed by two acrylic discs with two Kapton windows cut in the middle, accomplished by a working electrode connected with a gold wire current collector to reinforce the contact in the cell system via Pd gauze count electrode. Then the Hg/Hg_2SO_4 MMS reference electrode was connected to the electrochemical cell using a salt bridge, re-assembled to produce a sufficiently large absorption edge. The electrolyte was 2.5 mol dm^{-3} sulphuric acid (H_2SO_4) solution for a standard CV measurement and 1 mol dm^{-3} for the in-situ EXAFS measurement at a scan rate of 1 mV s^{-1} in a potential region of -0.675 V to 0.4 V, respectively, in which no solvent and electrolyte decomposition were detected [36].

2.3. The Extended X-ray Adsorption Fine Structure Measurement

The Pd electrocatalyst under investigation has low-level of concentration distribution on zeolite made of amorphous polymer material that has short-range order characteristics of electron scatting. Thus, the Pt particle structure investigation on zeolite is limited by standard measurement

methods. Subsequently, the EXAFS measurements were performed using a Synchrotron Radiation Source (SRS) at STFC Daresbury Laboratory, UK. The wiggler beam line was operated at conditions of 2 *GeV* and 100 *mA*. High-order harmonics that might affect the amplitude of EXAFS were removed using a double-crystal Si220 monochromator. The 50 % detuning of harmonic beam using gas ion chambers filled with Ar, Xe or Kr and He was used to locate the Pd K absorption edge under fluorescence mode. A Pd foil was used as a reference sample for EXAFS data collection.

Data analysis was carried out using in-house software EXCURV 98. The inter-atomic distance, atom number and the type of backscattering neighbors were determined using a method proposed by Abruna [37]. Therefore, the Pd particle local structure information such as number of atoms in a Pd cluster and Pd-Pd binding distance can be analyzed in a great detail.

3. Results and Discussion

3.1. Cyclic Voltammetry (CV) measurement in H_2SO_4 electrolyte solution

The CV measurement was performed to determine the electro-activity of species in the H_2SO_4 electrolyte solution and on Pd surface by monitoring the current density change against the potential.

Figure 2 depicts the electrochemical measurement for electrode made by 40 wt% Pd on XC-72R carbon using a scan rate of 20mV/s. The CV consists of a very clear electrochemical feature in the hydrogen re-adsorption (HRS) and hydrogen re-oxidation (HRO) regions, as verified by two separated quasi-reversible peaks that represents hydrogen adsorption and desorption peaks on Pd surface. The peaks 'A' and 'C' determined at -0.47 V and -0.647 V on the cathodic sweep are strongly associated with hydrogen adsorption site and hydrogen evolution, respectively, and a small peak 'B' observed at -0.53 V presents a weakly hydrogen adsorption site. The additional peak 'D' predicted at -0.63 V on the anodic sweep is attributed to the re-oxidation of H_2. The peak 'E' predicted at -0.442 V is due to weakly bond H desorption and the peak 'F' at -0.382 V is due to strongly bond H desorption, respectively. The current density increase between 0.176 V and 0.4 V in the anodic sweep are the re-

oxidation of the Pd surface (OR region), and a large peak 'G' determined at 0.079 V in the cathodic sweep is attributed to the removal of oxygen on Pd surface. The oxidation current density increases with the increase of potential in oxidation region up to 0.4 V.

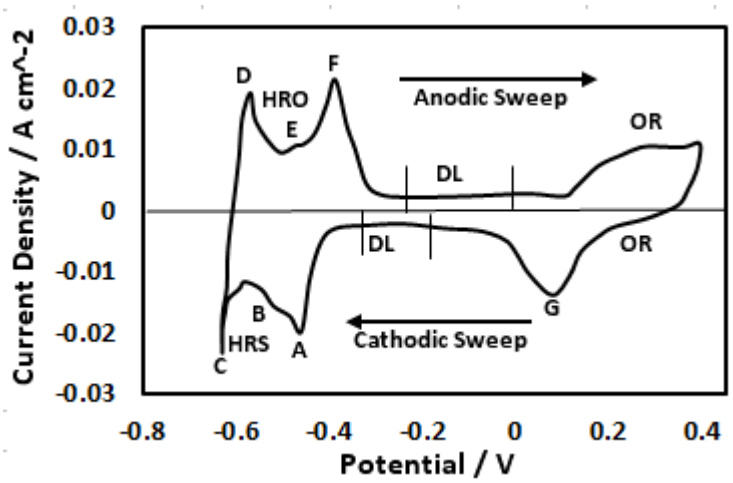

Figure 2. Steady state cyclic voltammogram measurement using a Nafion@ bound working electrode made by 40 wt% Pd on XC-72R carbon, scanned rate at 20 mV s^{-1} in 2.5 mol dm^{-3} H_2SO_4 at the potential region of -0.65 V to 0.4 V vs MMS reference electrode.

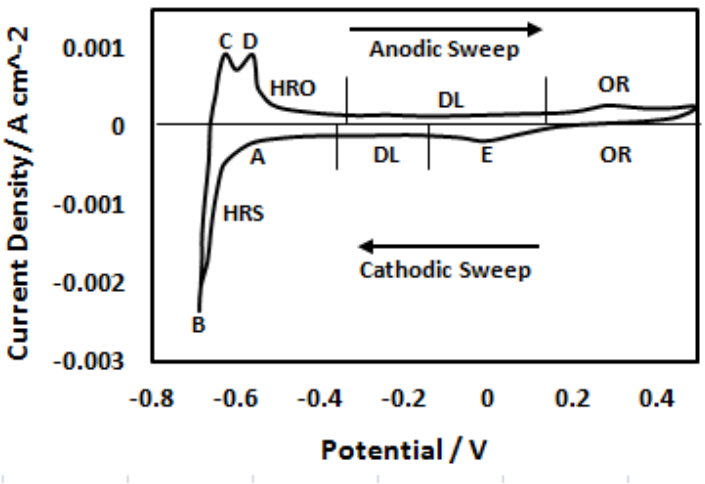

Figure 3. Steady state cyclic voltammogram measurement using 1.5 wt% Pd on XC-72R carbon powder Nafion@ bound working electrode made by 40 wt% Pd on XC-72R carbon electrocatalyst

241 mixed with extra carbon powder, scanned at 1 mV s^{-1} in 2.5 mol dm^{-3} H_2SO_4 at the potential region of
242 -0.675 V to 0.4 V vs MMS reference electrode.

243

244 Figure 3 displays cyclic voltammetry (CV) measurement for 1.5 wt% Pd on XC-72R carbon
245 Nafion@ bound working electrode made of 40 wt% Pd on XC-72R carbon electrocatalyst with extra
246 XC-72R carbon powder mixture (i.e. denoted as 15PdXC-72R). The CV consists of a very similar
247 electrochemical feature as that presented in Figure 2. The two distinguished regions are associated
248 with the hydrogen adsorption, evaluation, hydrogen desorption and the re-oxidation peaks,
249 respectively.

250 A double layer (DL) current density is measured at a potential region of -0.18 V to -0.420 V in the
251 cathodic sweep and 0.18 V to -0.4 V in the anodic sweep respectively. A small peak 'A' detected at -
252 0.59 V is correspondent to hydrogen adsorption on Pd surface, and hydrogen evolution (peak 'B') is
253 observed at -0.689 V. The peak 'C' at -0.626 V on the anodic sweep is related to hydrogen re-
254 oxidation and the second peak 'D' at -0.564 V is attributed to hydrogen desorption. The current
255 density increase from 0.226 V to 0.4 V is attributed to the formation of Pd oxide (PdO) on electrode
256 surface. A peak 'E' interpreting the striping of O formed on Pd surface is predicted at 0.0656 V.
257 The electrochemical activity of Pd on zeolite was determined using a Nafion@ bound Pd zeolite
258 electrode fabricated by 1.5 wt% Pd loading on zeolite with extra XC-72R carbon power. The 1.5 wt%
259 Pd zeolite sample was calcined at 350 ^{o}C in O_2 and reduced at 360 ^{o}C in 5 % hydrogen and 95 %
260 nitrogen (denoted as 15Pdanc35r36 thereafter).
261 CV measurement for electrode 15Pdanc35r36 presented in Figure 4 has shown three
262 distinguished features captured in hydride region. The hydrogen adsorption peak 'A' is predicted at -
263 0.644 V which is shifted to further negative than that by electrode 15PdXC-72R, and the second peak
264 'B' at -0.677 V is linked to hydrogen evaluation. The single peak 'C' detected at -0.604 V on the
265 anodic sweep is associated to hydrogen desorption. By comparison with the electrochemical

performance of electrode 15XC-72R, the electrode 15Pdanc35r36 presents a relatively high electrochemical activity, as interpreted by high current density change at hydride region. No hydrogen re-oxidation peak is observed at the potential region of -0.675 V. This may be due to the energy level for H_2 re-oxidation is very close to the energy required for hydrogen desorption.

An oxidation current density is observed between 0.109 V and 0.4 V, and the removal of oxygen on Pd surface is captured at 0.0198 V (peak 'D') during the cathodic sweep. Nevertheless, the electrocatalyst made of 1.5 wt% Pd using either zeolite or XC-72R carbon as substrate gives out a very different current density change of hydrogen adsorption and desorption features. This may be due to Pd particle size smaller on zeolite than on carbon support.

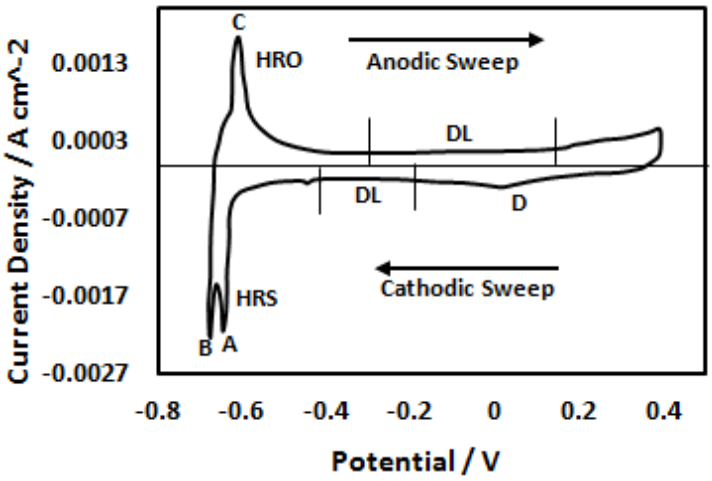

Figure 4. Steady state cyclic voltammogram measurement using 1.5 wt% Pd on zeolite with extra XC-72R carbon powder mixture Nafion@ bound working electrode (i.e. 15Pdanc35r36), scanned at a rate of 1 mV/s in 2.5 mol dm^{-3} H_2SO_4 at the potential region of -0.675 V to 0.4 V vs MMS reference electrode.

3.2. In-situ EXAFS study for 1.5 wt% Pd/Y zeolite electrocatalyst

The in-situ EXAFS data for a sample 15Pdanc35r36 was collected at the Pd K edge via a fluorescence mode under potential control of -0.675 V, -0.63 V, -0.5 V and 0.5 V, respectively, with

correspondent to an Hg/Hg_2SO_4 Mercury/Mercuries Sulphate (MMS) reference electrode. The resulting Chi data and their Fourier transforms are displayed in Figure 5.

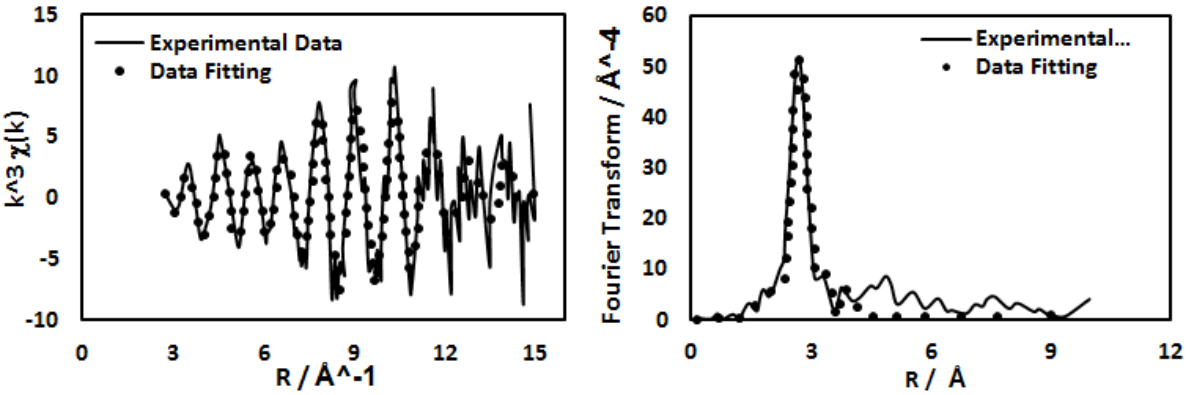

(a) -0.675 V

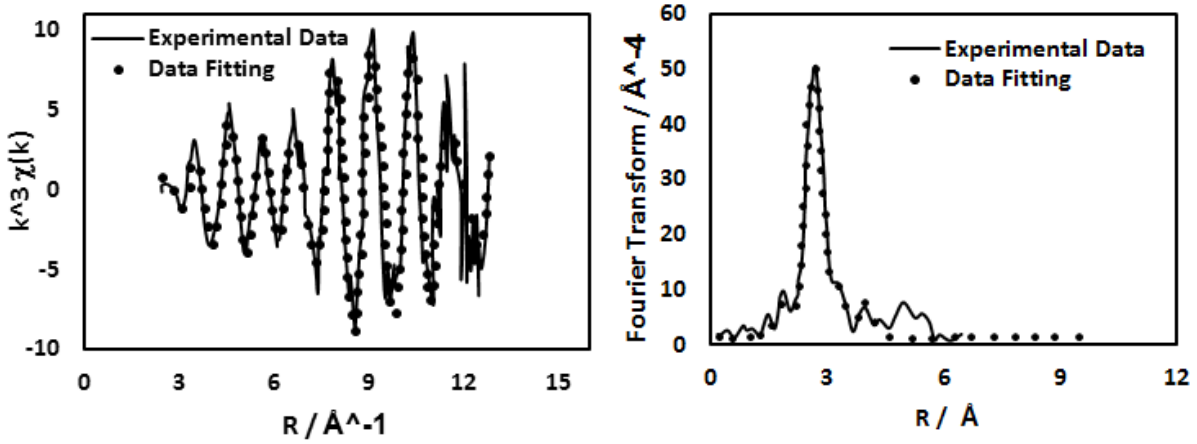

(b) -0.65 V

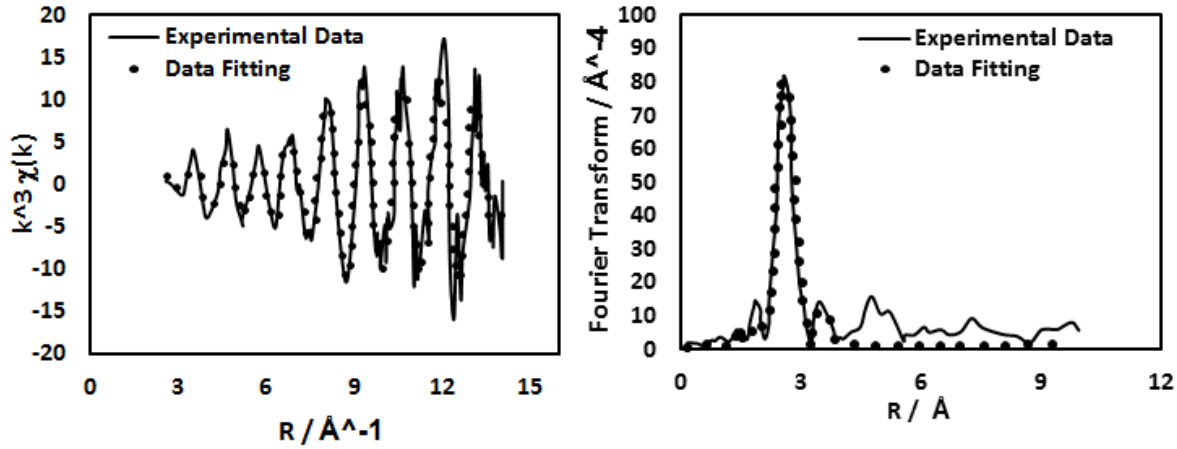

(c) -0.5 V

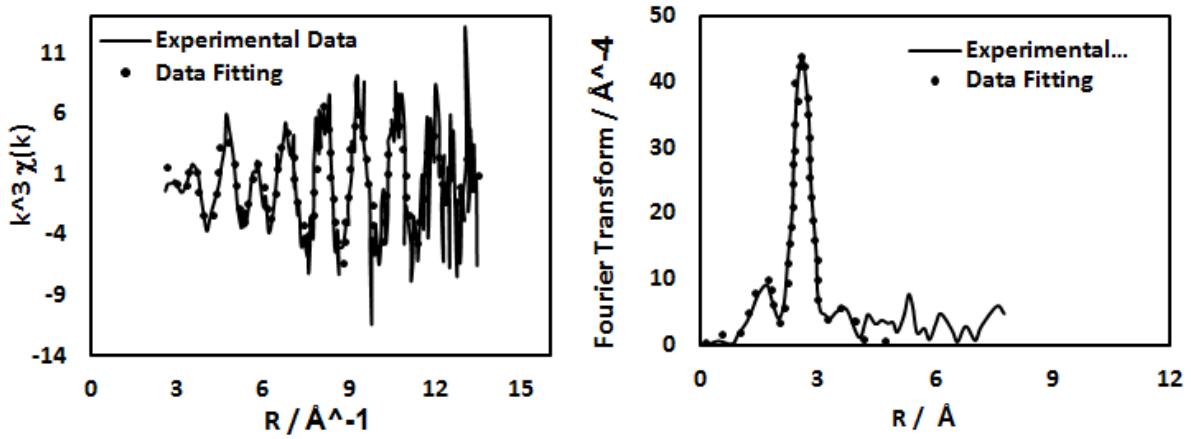

(d) +0.5 V

Figure 5. Chi data and Fourier transforms for 1.5 wt% Pd loading on zeolite catalyst calcined at 350 °C and reduced at 360 °C (i.e. 15Pdanc35r36), phase corrected. The data were collected at room temperature. The solid lines represent the experimental data and dashed lines represent the fitted data: (a) at -0.675 V; (b) at -0.65 V; (c) at -0.5 V; (d) at +0.5 V.

Table 1. The fitting results for each Pd shell

(a) EXAFS data fitted at the Pd K edge at -0.675 V vs MMS reference electrode

15Pdanc35r36	N	$2\sigma^2/Å^2$	R/ Å
Shell 1_Pd	7.86±0.46	0.0168±0.0007	2.83±0.005
Shell 2_Pd	0.58±0.25	0.0061±0.0031	3.46±0.019
Shell 3_Pd	4.74±0.26	0.0268±0.0080	4.00±0.036

(b) EXAFS data fitted at the Pd K edge at -0.65 V vs MMS reference electrode

15Pdanc35r36	N	$2\sigma^2/Å^2$	R/ Å
Shell 1_Pd	7.09±0.31	0.0151±0.0005	2.80±0.004
Shell 2_Pd	1.11±0.22	0.0049±0.0017	3.47±0.011
Shell 3_Pd	2.73±0.69	0.0127±0.0025	3.96±0.013

(c) EXAFS data fitted at the Pd K edge at -0.50 V vs MMS reference electrode

15Pdanc35r36	N	$2\sigma^2$/Å^2	R/ Å
Shell 1_Pd	5.65±0.61	0.0088±0.0005	2.74±0.005
Shell 2_Pd	2.42±0.54	0.0059±0.0036	3.80±0.024

(d) EXAFS data fitted at the Pd K edge at +0.50 V vs MMS reference electrode

15Pdanc35r36	N	$2\sigma^2$/Å^2	R/ Å
Shell 1_Pd	6.18±0.52	0.0162±0.0009	2.73±0.008
Shell 2_Pd	4.68±0.31	0.0419±0.0363	3.33±0.008
Shell 3_O	0.64±0.31	0.0272±0.0099	2.00±0.133

Chi data is extended until at k = 15 Å^{-1} for a potential at -0.675 V, k = 13 Å^{-1} for a potential at -0.65 V, k = 14 Å^{-1} for a potential at -0.5 V and k = 13.5 Å^{-1} for a potential at +0.5 V, respectively. All data were fitted using k^3 weighting and in r-space, and the fits are represented by dashed lines. The fitting parameters are summarized in table 1.

The Pd-Pd distance in the first shell of Pd-Pd is fitted approximately with 2.83 Å at -0.675 V and 2.8 Å at -0.65 V, respectively, that distance is slightly longer than 2.75 Å observed for the bulk of Pd. The Pd distance is fitted around 2.74 Å at -0.5 V and 2.73 Å at +0.5 V, respectively, which appears to be metallic in nature. The increase of Pd-Pd distance at a negative potential over -0.5 V may be attributed by hydrogen atoms that are not only absorbed on the Pd surface but also forms Pd hydride phases, i.e. β-PdH or α-PdH on Pd, through an H atom migration process such as hydrogen spillover or surface conductance [38]. In electrochemical environment, β-PdH is associated with a direct hydrogen adsorption reaction between electrode surface and sub-surfaces, while α-PdH may be formed by H migration from a nearer surface of hydride phase to the centre of metal particle. The hydrogen transfer between α-PdH and β-PdH to Pd may be attributed by up-hill diffusion from

decomposition of β-PdH layer into α-PdH, whereas hydrogen in the α-PdH layer is decomposed and transferred into the Pd [4, 38]. Both CV measurement and EXAFS data analysis indicate that the Pd electrochemical activity is associated with the location of Pd on zeolite. An O shell with coordination number of 0.64 was predicted at 0.5 V. The Pd-O distance was fitted at 2 Å, consistent to the value observed for Pd metal oxides (see table 1d).

The number of Pd coordination predicted is dependent on potential regime. The large Pd coordination number was fitted at -0.675 V, -0.65 V and +0.5 V, respectively. This can result in a low Pd active surface area which has indicated by small hydrogen adsorption peak, compared to that predicted at -0.5 V. The Pd coordination numbers were fitted with low values at -0.5 V, indicting Pd particle size was small. The change of Pd coordination number at different potential regimes can be interpreted that Pd seems more mobile than Pt in zeolite structure. This may be due to their d bond electron configuration [13, 25]. The valence electrons on Pd are located in the 4d orbit, whilst electrons on Pt are in the 5d orbit. Additionally, Pd^{2+} ion has greater charge density than Pt^{2+}.

The CV measurement for 1.5 wt% Pd/Y zeolite sample has shown same basic current density change features observed for 40 wt% Pd/C catalyst, represented by hydrogen adsorption and evaluation, desorption and re-oxidation peaks. However, there is no clear visible hydrogen desorption feature observed for 1.5 wt% Pd/C sample made by 40 wt% Pd/C and extra XC-72R carbon mixture. This is probably because that the Pd active surface area on XC-72R carbon might be smaller than that on zeolite.

The number of Pd atoms for catalyst sample 15Pdanc35r36 is predicted at approximately 12 using Benfield model [39]. The Pd location is dependent on calcinations and reduction temperature [6]. The majority of Pd particle for 1.5 wt% Pd loading on zeolite calcined at 350 ^{o}C and reduced at 360 ^{o}C (i.e. 15Pdanc35r36) are more likely to reside at the zeolite sodalite cage. A temperature higher than 360 ^{o}C is required to remove Pd nanoparticle from sodalite cage to the zeolite supercage or zeolite external surface. This might be attributed by Pd and zeolite substrate interaction that is able dramatically to modify the density of energy on Pd cluster. In order to further understanding Pd

behavior within zeolite channels, future work could focus on following topics as: (1) the Pd mobility and Pd particle interaction with zeolite structure using excess H^+ ions exchanged into zeolite active sites; (2) the increase of Pd performance by forming Pd metal alloys under various calcinations and reduction temperature conditions; and (3) the efficiency of small organic molecules such as formic acid and methanol oxidation on Pd electrocatalysts.

4. Conclusions

This paper presents the characteristics of zeolite supported 1.5 wt% Pd nanoparticle made by ion exchange method. The Pd electrocatalytic performances are characterized by EXAFS analysis and Cyclic Voltammetry measurements. In general, the Pd electrochemical activity depends on the Pd location and particle size. CV measurements indicate that Pd metal particles on the external of zeolite surface or inside zeolite supercage can be electrochemically accessible and reduced. EXAFS fitting results have interpreted Pd particle size on zeolite at different potential regions ranked in an order of -0.675 V > -0.65 V > 0.5 V > -0.5 V. This also results in Pd active surface areas ranked at the potential region in an order of -0.5 V > 0.5 V > -0.65 V > -0.675 V. The Pd distance is larger than 2.75 Å at the potential region between -0.675 V and -0.65 V. This might be attributed by either electrochemical adsorption of H atom on the Pd active surface forming Pd hydride phases, i.e. β-PdH by direct hydrogen adsorption on electrode surface or α-PdH by migration of H atom onto Pd surface. The Pd appears to be more metallic in nature at $\pm$0.5 V, whereas Pd distance is consistent in comparison of bulk Pd. The Pd may be electronically accessible via hydrogen spillover or surface conductance.

A further study can be carried out to investigate the Pd electrochemical activity in connection with Pd particle size with correspondent to Pd zeolite catalyst pre-treatment condition under different calcinations and reduction temperatures. The Pd particle performance will be characterized via electrooxidation of small organic molecules on Pd surface, e.g. formic acid and methanol, among other materials.

5. References

[1] Zhang L, Chang Q, Chen H, Shao M. Recent advances in palladium-based electrocatalysts for fuel cell reactions and hydrogen evolution reaction. Nano Energy 2016; 29: 198-219.

[2] Shao M. Palladium-based electrocatalysts for hydrogen oxidation and oxygen reduction reactions. J. Power Sources 2011; 196(5): 2433-2444.

[3] Shi Z, Szpunar JA. Synthesis of an Ultra-Thin Palladium Membrane for Hydrogen Extraction. Review on Advanced Materials Science 2007; 15(1): 1-9.

[4] Wilde M, Matsumoto M, Fukutani K, Aruga T. Depth-resolved analysis of subsurface hydrogen absorbed by Pd(1 0 0). Surface Science 2001; 482-485(Part 1): 346-352.

[5] Yao S, Li G, Liu C, Xing W. Enhanced catalytic performance of carbon supported palladium nanoparticles by in-situ synthesis for formic acid electrooxidation. J. of Power Sources 2015; 284: 355-360.

[6] Ghasemi S, Hosseini SR, Nabipour S, Asen P. Palladium nanoparticles supported on graphene as an efficient electrocatalyst for hydrogen evolution reaction. Int. J. of Hydrogen Energy 2015; 40(46): 16184-16191.

[7] DÖner A, Tezcan F, Kardas G. Eelectrocatalytic behavior of the Pd-modified electrocatalyst for hydrogen evolution. Int. J. Hydrogen Energy 2013; 38(10): 3881-3888.

[8] Ojani R, Raoof JB, Hasheminejad E. One-step electroless deposition of Pd/Pt bimetallic microstructures by galvanic replacement on copper substrate and investigation of its performance for the hydrogen evolution reaction. Int. J. Hydrogen Energy 2013; 38(1): 92-99.

[9] Safavi A, Kazemi SH, Kazemi H. Electrocatalytic behaviors of silver-palladium nanoalloys modified carbon ionic liquid electrode towards hydrogen evolution reaction. Fuel 2014; 118: 156-162.

[10] Homeyer ST, Sachtler WMH. Elementary steps in the formation of highly dispersed palladium in NaY: I. Pd ion coordination and migration. Journal of Catalysis 1989; 117(1): 91-101.

[11] Yan Z, Zhang M, Xie J, Zhu J, Shen PK. A bimetallic carbide Fe2MoC promoted Pd electrocatalyst with performance superior to Pt/C towards the oxygen reduction reaction in acidic media. Applied Catalysis B: Environmental 2015; 165: 636-641.

[12] Xia M, Ding W, Xiong K, Li L, Qi X, Chen S, Hu B, Wei Z. Anchoring Effect of Exfoliated-Montmorillonite-Supported Pd Catalyst for the Oxygen Reduction Reaction. The J. Phys. Chem. C 2013; 117(20): 10581-10588.

[13] Sachtler WMH, Zhang ZC. Zeolite-supported transition metal catalysts. Advances in Catalysis 1993; 39: 129-220.

[14] Tzou MS, Teo BK, Sachtler WMH. Formation of Pt particles in Y-type zeolites: The influence of coexchanged metal cations. Journal of Catalysis 1988; 113(1): 220-235.

[15] Xu L, Zhang Z, Sachtler WMH. Effect of zeolite protons on Pd particle size and H_2 chemisorption. Journal of the Chemical Society Faraday Transitions 1992; 88(15): 2291-2295.

[16] Zhao X, Hu Y, Liang L, Liu C, Liao J, Xing W. Ionic liquid-mediated synthesis of 'clean' palladium nanoparticles for formic acid electrooxidation. Int. J. Hydrogen Energy 2012; 37(1): 51-58.

[17] Vijwani H, Mukhopadhyay SM. Palladium nanoparticles on hierarchical carbon surfaces: A new architecture for robust nano-catalysts. Applied Surface Science 2012; 263: 712-721.

[18] Hammer B, Special sites at noble and late transition metal catalysts. Topics in Catalysis 2006; 37(1): 3-16.

[19] Suarez-Alcantara K, Martinez-Casillas DC, Zheng KB, Zhu Q, Abdellah M, Haase D, Pullerits T, Solorza-Feria O, Canton SE. SEM and XAS characterization at beginning of life of Pd–based cathode electrocatalysts in PEM fuel cells. Int. J. Hydrogen Energy 2014; 39(10): 5358-5370.

[20] Baldauf M, Kolb DM. A hydrogen adsorption and absorption study with ultrathin Pd overlayers on Au(111) and Au(100). Electrochimica Acta 1993; 38: 2145 – 2153.

[21] Eftekhari A. Electrocatalysts for hydrogen evolution reaction. Int. J. Hydrogen Energy 2017 (in press); http://dx.doi.org/10.1016/j.ijhydene.2017.02.125.

[22] Quaino P, Santos E, Wolfschmidt H, Montero MA, Stimming U. Theory meets experiment: Electrocatalysis of hydrogen oxidation/evolution at Pd–Au nanostructures. Catal. Today 2011; 177(1): 55-63.

[23] Pandelov S, Stimming U. Reactivity of monolayers and nano-islands of palladium on Au(1 1 1) with respect to proton reduction. Electrochimica Acta 2007; 52(18): 5548-5555.

[24] Conway BE, Tilak BV. Interfacial processes involving electrocatalytic evolution and oxidation of H2, and the role of chemisorbed H. Electrochimica Acta 2002; 47(22-23): 3571-3594.

[25] Yao J, Yao Y. Experimental study of characteristics of bimetallic Pt–Fe nano-particle fuel cell electrocatalyst. Renewable Energy 2015; 81: 182-196.

[26] Bianchini C, Shen PK. Palladium-Based Electrocatalysts for Alcohol Oxidation in Half Cells and in Direct Alcohol Fuel Cells. Chem. Rev. 2009; 109(9): 4183-4206.

[27] Damjanovic A, Brusic V. Oxygen reduction at Pt-Au and Pd-Au alloy electrodes in acid solution. Electrochimica Acta 1967; 12(9): 1171-1184.

[28] Kondo S, Nakamura M, Maki N, Hoshi N. Active Sites for the Oxygen Reduction Reaction on the Low and High Index Planes of Palladium. The Journal Physical Chemistry C 2009; 113(29): 12625-12628.

[29] Shao M, Yu T, Odell JH, Jin M, Xia Y. Structural dependence of oxygen reduction reaction on palladium nanocrystals. Chemical Communications 2011; 47: 6566-6568.

442 [30] Stassi A, Gatto I, Baglio V, Arico AS. Evaluation of Palladium–based electrocatalyst for oxygen
443 reduction and hydrogen oxidation in intermediate temperature polymer electrolyte fuel cells. Int. J.
444 Hydrogen Energy 2014; 39(36): 21581-21587.

445 [31] Han W, Kwan SM, Yeung LK. Zeolite application in fuel cell: water management and proton
446 conductivity. Chemical Engineering Journal 2012; 187: 367-371.

447 [32] Caro J, Noack M, Kolsch P, Schafer R. Zeolite membranes – state of their development and
448 perspective. Microporous Mesoporous Materials 2000; 38(1): 3-24.

449 [33] Pandya KI, Heald SM, Hriljac JA, Petrakis L, Fraissard J. Characterization by EXAFS, NMR, and
450 Othe Technique of Pt/NaY Zeolite at Industrially Relevant Low Concentration of Platinum. The
451 Journal of Physical Chemistry 1996; 100(12): 5070-5077.

452 [34] Yao J, Yao YF. Investigation of zeolite supported platinum electrocatalyst for electrochemical
453 oxidation of small organics species. Int. J. Hydrogen Energy 2016; 41(33): 14747-14757.

454 [35] Bergeret G, Gallezot P, Imelik B. X-ray study of the activation, reduction, and re-oxidation of
455 palladium in Y-type zeolites. J. Phys. Chem. 1981; 85(4): 411-416.

456 [36] Brett CMA, Brett AMO. Electroanalysis. 1998: Oxford University Press.

457 [37] Abruna HD. X-ray absorption spectroscopy in the study of electrochemical system. In: HD
458 Abruna (Eds.), Electrochemical interface: modern techniques for in-Situ interface characterization.
459 New York: VCH Publishers; 1991, Chapter 1: pp.1-54

460 [38] Yang TH, Pyun SI, Yoon YG. Hydrogen transport through Pd electrode: current transient analysis.

461 Electrochimica Acta 1997; 42(11): 1701-1708.

462 [39] Benfield RE. Mean coordination numbers and the non-metal-metal transition in cluster. J. of the
463 Chem. Soc. Faraday Trans. 1992; 88(8): 1107-1110.